

Pure spin currents in Ge probed by inverse spin-Hall effect

F. Bottegoni,^{a)} C. Zucchetti, M. Finazzi, G. Isella, and F. Ciccacci

LNES-Dipartimento di Fisica, Politecnico di Milano, Piazza Leonardo da Vinci 32, 20133 Milano, Italy

(Dated: 2 September 2016)

We perform photoinduced inverse spin-Hall effect (ISHE) measurements on a Pt/Ge(001) junction at room temperature. The spin-oriented electrons are photogenerated at the Γ point of the Ge Brillouin zone using circularly-polarized light. After the ultrafast $\Gamma - L$ scattering in the Ge conduction band, electrons diffuse into the Pt layer where spin-dependent scattering with Pt nuclei yields a transverse electromotive field E_{ISHE} . The ISHE signal dependence as a function of the incident photon energy is investigated and interpreted in the frame of a one-dimensional spin drift-diffusion model. This allows estimating the electron spin lifetime at the L -valleys to be $\tau_s = 1$ ns.

The study of spin injection and transport in semiconductors lies at the core of spintronics.¹ An efficient tool to generate spin populations in semiconductors is represented by optical orientation.² In this technique, dipole selection rules for optical transitions with circularly-polarized light allows for the injection of a spin-oriented electron population in the conduction band of the semiconductor with a spin polarization $P = (n_{\uparrow} - n_{\downarrow}) / (n_{\uparrow} + n_{\downarrow})$, being $n_{\uparrow(\downarrow)}$ the up-(down-) spin densities referred to the quantization axis given by the direction of light propagation in the material.

Spin-orbit interaction plays a fundamental role in this process, removing the energy degeneracy between heavy and light holes (HH and LH) states and split off (SO) states at the Γ point of the semiconductor Brillouin zone. A net electron spin polarization is then achieved when the photon energy is tuned to the direct bandgap and electrons coming only from HH and LH states are promoted to the conduction band.

The first demonstration of optical orientation was done in Si:³ however, the small energy splitting $\Delta E_{\text{so}} = 44$ meV between HH-LH and SO states at Γ and the indirect nature of the Si electronic gap have prevented further optical investigations on bulk Si and promoted, on the other hand, many studies on Ge and GaAs, which are characterized by a higher spin-orbit interaction ($\Delta E_{\text{so}} = 0.29$ and 0.34 eV for Ge and GaAs, respectively). In this materials optically-injected spin currents can reach spin polarization values up to 50% in bulk semiconductors⁴⁻⁸ or even larger in semiconductor nanostructures.⁸⁻¹⁶

In this respect it would be highly desirable to implement the control of the spin degree of freedom in Ge-based heterostructures, which can be integrated on the common Si-based electronics platform. In bulk Ge the energy difference between direct ($E_d = 0.80$ eV) and indirect ($E_i = 0.66$ eV) bandgap is only 140 meV at room temperature. This means that electrons photo-excited close to the Γ point undergo a fast thermalization to the L -valleys within about 300 fs so that the electron transport in Ge generally occurs at the indirect gap.¹⁷ The

$\Gamma - L$ scattering partially preserves the initial electron spin, as observed in low-temperature spin-resolved photoluminescence measurements.¹⁸ Moreover, in the past years, spin pumping experiments at room temperature have demonstrated the possibility to achieve spin accumulation in the Ge conduction band,¹⁹ which can be consequently detected inside Ge by means of inverse spin-Hall effect.²⁰ The relatively long electron spin-lifetimes, predicted^{21,22} and experimentally measured²³⁻²⁶ in Ge, together with the “quasi direct” bandstructure of Ge, make this material a promising candidate for the implementation of devices where spins are optically injected and electrically detected.

In the following, we will show that an optically-injected spin current can be generated in the Ge conduction band and detected by means of a thin Pt layer, grown on top of the bulk Ge substrate. Spin polarized electrons entering the Pt film from the semiconductor undergo spin-dependent scattering events which result in transverse electromotive field E_{ISHE} at the edge of Pt, a process known as inverse spin-Hall effect (ISHE).²⁷ We will discuss the photon energy dependence of the ISHE signal by exploiting a one-dimensional spin-drift diffusion model which allows for the estimation of the electron spin lifetime at the L -valleys.

The sample structure together with the experimental geometry are sketched in Fig. 1a. A $l_x \times l_y = 5 \times 5$ mm² 4 nm-thick Pt layer is deposited by e-beam evaporation on a 450 μm -thick As-doped Ge(001) substrate ($N_D = 1.7 \times 10^{16}$ cm⁻³). Two 50 nm-thick Au/Ti contacts are evaporated at the edges of the Pt layer in order to measure the electromotive force produced by the ISHE process in Pt.

ISHE measurements were performed at room temperature. The sample was illuminated with a collimated monochromatic beam with a spot size $d \approx 4$ mm from a Ti-sapphire tunable laser, which provides photons in the spectral range from 1.2 to 1.8 eV. Two CW lasers were used for ISHE measurements at 1 and 0.8 eV excitation energy. We exploited a photo-elastic modulator (PEM) operating at 50 kHz to modulate the light circular polarization. The differential electromotive force ΔV between the two Au electrodes (see Fig. 1a) was de-

^{a)}Electronic mail: federico.bottegoni@mail.polimi.it

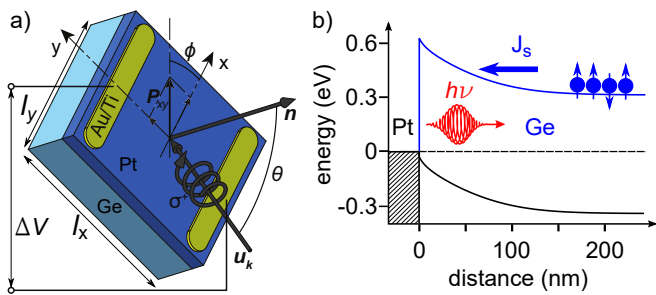


FIG. 1: (Color online) (a) Sketch of the Pt/Ge(001) sample and the experimental geometry: θ is the angle between the direction of the incident light \mathbf{u}_k and the normal \mathbf{n} to the sample surface, whereas φ is the angle between the projection of \mathbf{u}_k in the sample plane and the x axis. (b) Pt/Ge Schottky junction and band alignment at the Pt/Ge interface: under illumination with circularly-polarized light and open-circuit conditions, a spin current density J_s is generated in the Ge conduction band, flowing toward the Pt/Ge interface along the L -valleys. The measured Schottky barrier height is $E_B = 0.62$ eV, in good agreement with the reported values of Ref. 28

tected by a lock-in amplifier. The sample was mounted on a multi-axial stage, which allowed the rotation of the sample around the polar angle θ and the azimuthal angle φ , defined in Fig. 1a.

The optical orientation process generates spin-polarized electron-hole pairs around the Γ point of the Brillouin zone. Due to the fact the hole spin lifetime is in the fs range,²⁹ it is a good approximation to consider the holes completely depolarized right after the photocreation, so that most of the spin current density J_s , flowing into the Ge substrate, is carried by spin-oriented electrons. Moreover, due the optical orientation process does not inject any net charge in the semiconductor, but the two electron spin populations are unbalanced, a pure spin current is generated into Ge. As a consequence of the ultrafast $\Gamma - L$ scattering in the Ge conduction band, spin-oriented electrons diffuse along the L -valleys toward the Pt layer. The Pt/Ge interface has been electrically characterized by measuring the I-V curves (not shown) from a similar Pt/Ge junction, where an ohmic AgSb back contact was grown on the Ge substrate. The height of Schottky barrier is $E_B = 0.62$ eV, as indicated in Fig. 1b, in agreement with reported values of Ref. 28.

When entering the Pt layer, spin-oriented electrons scatter with Pt nuclei: as a consequence, a transverse voltage difference ΔV is measured at the edges of the Pt film, where $\Delta V = E_{\text{ISHE}} \cdot d$ and $\mathbf{E}_{\text{ISHE}} = D_{\text{ISHE}}(\mathbf{J}_s \times \mathbf{P})$,²⁷ being D_{ISHE} a constant representing the efficiency of the ISHE process. Due to the fact that \mathbf{J}_s can be assumed to be perpendicular to the Pt/Ge interface and we can detect only the component of \mathbf{E}_{ISHE} along the y -axis (which is the direction connecting the two Au/Ti contacts), the Pt/Ge junction is illuminated

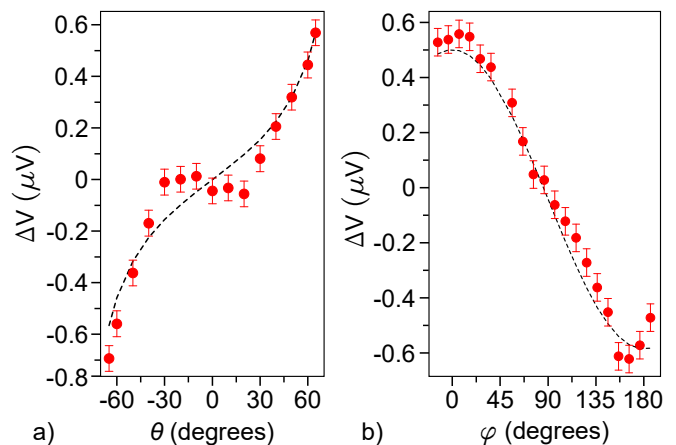


FIG. 2: (Color online) ISHE signal dependence as a function of (a) the angle θ for fixed $\varphi = 0^\circ$ and (b) of the angle φ for a fixed $\theta = 65^\circ$. The measurements have been performed at room temperature with a photon energy $h\nu = 1.77$ eV and an incident power $W = 230$ mW. The black dashed line corresponds to the $\cos \beta \tan \theta$ -dependence (a) and $\cos \varphi$ -dependence (b), as obtained from a multilayer optical analysis of the Pt/Ge sample.

at grazing incidence in order to maximize the P_x component of the photoinduced spin polarization vector \mathbf{P} (see Fig. 1a).

Indeed, the spin-related origin of the detected voltage difference ΔV can be verified by varying the P_x component of the interfacial plane projection \mathbf{P}_{xy} . Fig. 2a shows the ΔV dependence as a function of the angle θ for $\varphi = 0$, an incident photon energy $h\nu = 1.77$ eV and an incident power $W = 230$ mW. A noise voltage slightly lower than 100 nV, identified by the error bars, was detected for all the experimental points. The maximum ISHE signal $\Delta V = 0.6 \mu\text{V}$ is obtained for $\theta = 65^\circ$, in agreement with photoinduced ISHE measurements of Ref. 30. The θ -dependence of the ISHE signal can be completely explained considering a multilayer optical analysis on the Pt/Ge junction. Indeed $\Delta V(\theta, \varphi) \propto t_s t_p \cos \beta \cos \varphi \tan \theta$,^{30,31} being $t_{s(p)}$ the Fresnel coefficient of the $s(p)$ -polarized light and β the angle between the light propagation wavevector inside the Ge substrate and the normal to the sample surface. Taking into account an incident photon energy $h\nu = 1.77$ eV, we have exploited the Fresnel coefficients of Refs. 32 and 33 for Pt and Ge, respectively. In this case, it is possible to directly calculate the dependence of ΔV on θ (black dashed line in Fig. 2a) and φ (black dashed line in Fig. 2b) in order to compare the calculated behaviour to the experimental dataset in Fig. 2. We found a fair agreement between the theoretical calculations and the experiments, which ensures the spin-related origin of the measured signal.^{26,34}

Fig. 3a shows the ISHE signal, normalized with respect to the photon flux, as a function of the incident

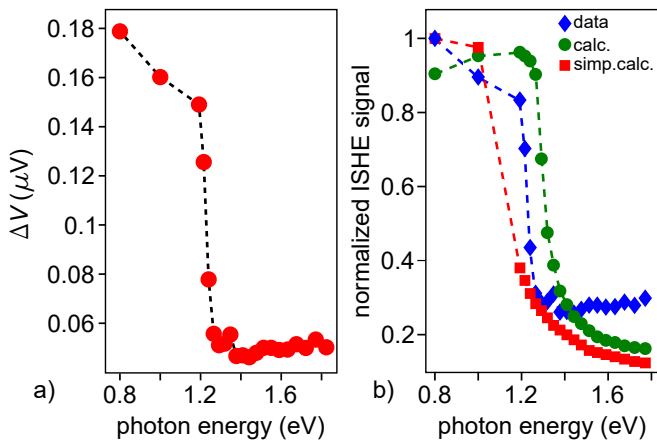


FIG. 3: (Color online) (a) ISHE signal dependence as a function of the incident photon energy, normalized with respect to the incident photon flux for $\theta = 65^\circ$ and $\varphi = 0$ in the 0.8-1.8 eV range. (b) Comparison between the measured electromotive force ΔV and the calculated spin current density J_s as a function of the incident photon energy. Calc and simple calc are related to the solution of Eqs. 1 and Eq. 2 for $\tau_s = 1$ ns, respectively.

photon energy in the 0.8-1.8 eV range. The behaviour of ΔV nicely resembles the dependence of the electron spin polarization P as a function of the incident photon energy.^{7,8,35} The maximum ISHE signal is obtained for $h\nu = 0.8$ eV, i.e. when the photon energy is resonant to the Ge direct gap, which indeed corresponds to the maximum initial electron spin polarization $P = 50\%$.³⁵ A sharp decrease is instead detected when approaching $h\nu = 1.1$ eV due to the fact that excitation energies well above the split-off threshold are achieved.^{34,36} Then, the further decrease, obtained when $h\nu > E_d + \Delta E_{so}$, is consistent with the strong decrease of the electron spin polarization \mathbf{P} .³⁵

The $h\nu$ -dependence of the experimental data can be explained by taking into account a one-dimensional spin-drift diffusion model.³⁷ In this respect, we have numerically solved the spin drift-diffusion equations for spin and charge at the Pt/Ge Schottky junction.³⁸ Under the approximation that only electrons are polarized and defining the spin density $s = n_\uparrow - n_\downarrow$, the spatial distribution of s and J_s can be described through the equations

$$\frac{1}{q} J_s(x) = -D_n \frac{\partial s(x)}{\partial x} - \mu_n s(x) E(x), \quad (1a)$$

$$\frac{1}{q} \frac{\partial J_s(x)}{\partial x} = -\frac{s(x)}{\tau_s} - w(x) s(x) p(x) + P\Phi\alpha e^{-\alpha x}. \quad (1b)$$

The electric field $E(x)$, hole density $p(x)$ and the intrinsic generation-recombination rate $w(x)$ can be calculated by numerically solving the coupled Poisson drift-diffusion equations³⁹ for electrons-holes pairs, which are

photogenerated by the incident photon flux. The electron mobility μ_n , diffusion coefficient D_n and Shockley-Read-Hall recombination parameters, which are used for the calculation of $w(x)$, correspond to typical values, also exploited for micro-electronic device simulations.⁴⁰ The absorption coefficient α and initial degree of electron spin polarization P are obtained from Refs. 33 and 35. Eqs. 1 describe the spin density s and the spin current density J_s profile along the axis perpendicular to the sample surface under steady-state conditions at the L -valleys of Ge, considering all the electrons thermalized. It is then assumed that the electron spin lifetime τ_s , which represents a free parameter in the solution of Eqs. 1, does not depend on $h\nu$. Furthermore the value of the spin polarization P after the $\Gamma - L$ scattering has been considered equal to the initial spin polarization.⁴¹ It is interesting to point out that a simplified solution of Eqs. 1 can be written as:

$$J_s = e\Phi P (1 - e^{-\alpha L_s}) \quad (2)$$

where e is the electron charge, Φ the photon flux and $L_s = \sqrt{D_n \tau_s}$ the spin diffusion length. At this point it is noteworthy to compare (see Fig. 3b) the experimental data of Fig. 3a and the spin current density J_s (which is proportional to the detected signal ΔV) at the Pt/Ge interface, as obtained from Eqs. 1 (calc. in Fig. 3b) and Eq. 2 (simp. calc. in Fig. 3b) with the choice $\tau_s = 1$ ns. The fair agreement between the calculations and the experiments indicates that the simple one-dimensional drift-diffusion model above is able to highlight the fundamental issues of spin transport at the L -valleys of Ge.

The reason why J_s (or ΔV) reproduces the energy dependence of the electron spin polarization P can be understood considering the simplified solution of Eq. 2, where it is basically assumed that all the spin-oriented electrons, generated within L_s from the Pt/Ge interface, are injected into the Pt layer without any spin relaxation. Within the whole investigated energy range $\alpha L_s \gg 1$: this means that all the photogenerated spins can reach the Pt/Ge interface without completely depolarizing, so that the decrease of the ISHE signal is only dictated by the energy dependence of the spin polarization profile.³⁷ This also explains the fact that the simplified model better reproduces the experimental data for $h\nu \approx E_d$, where most of the photoexcited spin-polarized electrons are created outside the depletion region.

In summary, we have shown that the optical orientation process can generate at room temperature a pure spin current in bulk Ge, which can be further detected through inverse spin-Hall effect by using a thin Pt layer. The dependence of the ISHE signal as a function of the incident photon energy has been explained in the frame of a one-dimensional spin-drift diffusion model, allowing the estimation of the electron spin lifetime at the L -valleys of Ge $\tau_s = 1$ ns. These results provide an important contribution for the development of Ge-based devices exploiting photoinduced spin currents.

ACKNOWLEDGMENTS

Partial funding is acknowledged to the CARIPLO project SEARCH-IV (grant 2013-0623).

- ¹I. Žutić, J. Fabian, and S. Das Sarma, *Rev. Mod. Phys.* **76**, 323 (2004), arXiv:0405528 [cond-mat].
- ²F. Meier and B. P. Zakharchenya, eds., *Optical orientation (Modern Problems in Condensed Matter Sciences, Vol. 8)* (Elsevier, Amsterdam, 1984) p. 523.
- ³G. Lampel, *Phys. Rev. Lett.* **20**, 491 (1968).
- ⁴R. Parsons, *Phys. Rev. Lett.* **23**, 1152 (1969).
- ⁵D. Pierce and F. Meier, *Phys. Rev. B* **13**, 5484 (1976).
- ⁶F. Ciccacci, *J. Appl. Phys.* **53**, 4395 (1982).
- ⁷R. Allenspach, F. Meier, and D. Pescia, *Phys. Rev. Lett.* **51**, 2148 (1983).
- ⁸F. Bottegoni, G. Isella, S. Cecchi, and F. Ciccacci, *Appl. Phys. Lett.* **98**, 242107 (2011).
- ⁹S. F. Alvarado, *Appl. Phys. Lett.* **39**, 615 (1981).
- ¹⁰F. Ciccacci, H.-J. Drouhin, C. Hermann, R. Houdre, and G. Lampel, *Appl. Phys. Lett.* **54**, 632 (1989).
- ¹¹T. Nakanishi, *Phys. Lett. A* **158**, 345 (1991).
- ¹²T. Maruyama, E. Garwin, R. Prepost, G. Zapalac, J. Smith, and J. Walker, *Phys. Rev. Lett.* **66**, 2376 (1991).
- ¹³Y. A. Mamaev, L. G. Gerchikov, Y. P. Yashin, D. A. Vasiliev, V. V. Kuzmichev, V. M. Ustinov, A. E. Zhukov, V. S. Mikhrin, and A. P. Vasiliev, *Appl. Phys. Lett.* **93**, 081114 (2008).
- ¹⁴F. Bottegoni, A. Ferrari, G. Isella, M. Finazzi, and F. Ciccacci, *Phys. Rev. B* **85**, 245312 (2012).
- ¹⁵F. Bottegoni, A. Ferrari, G. Isella, S. Cecchi, M. Marcon, D. Chrastina, G. Trezzi, and F. Ciccacci, *J. Appl. Phys.* **111**, 063916 (2012).
- ¹⁶a. Ferrari, F. Bottegoni, G. Isella, S. Cecchi, and F. Ciccacci, *Phys. Rev. B* **88**, 115209 (2013).
- ¹⁷X. Zhou, H. van Driel, and G. Mak, *Phys. Rev. B* **50**, 5226 (1994).
- ¹⁸F. Pezzoli, F. Bottegoni, D. Trivedi, F. Ciccacci, A. Giorgioni, P. Li, S. Cecchi, E. Grilli, Y. Song, M. Guzzi, H. Dery, and G. Isella, *Phys. Rev. Lett.* **108**, 156603 (2012).
- ¹⁹a. Jain, J.-C. Rojas-Sanchez, M. Cubukcu, J. Peiro, J. Le Breton, E. Prestat, C. Vergnaud, L. Louahadj, C. Portemont, C. Ducruet, V. Baltz, A. Barski, P. Bayle-Guillemaud, L. Vila, J.-P. Attané, E. Augendre, G. Desfonds, S. Gambarelli, H. Jaffrès, J.-M. George, and M. Jamet, *Phys. Rev. Lett.* **109**, 106603 (2012).
- ²⁰J.-C. Rojas-Sánchez, M. Cubukcu, A. Jain, C. Vergnaud, C. Portemont, C. Ducruet, A. Barski, A. Marty, L. Vila, J.-P. Attané, E. Augendre, G. Desfonds, S. Gambarelli, H. Jaffrès, J.-M. George, and M. Jamet, *Phys. Rev. B* **88**, 064403 (2013).
- ²¹J.-M. Tang, B. T. Collins, and M. E. Flatté, *Phys. Rev. B* **85**, 045202 (2012).
- ²²P. Li, Y. Song, and H. Dery, *Phys. Rev. B* **86**, 085202 (2012).
- ²³C. Guite and V. Venkataraman, *Phys. Rev. Lett.* **107**, 166603 (2011).
- ²⁴C. Hautmann, B. Surrer, and M. Betz, *Phys. Rev. B* **83**, 161203 (2011).
- ²⁵J. Lohrenz, T. Paschen, and M. Betz, *Phys. Rev. B* **89**, 121201 (2014).
- ²⁶F. Bottegoni, A. Ferrari, F. Rortais, C. Vergnaud, A. Marty, G. Isella, M. Finazzi, M. Jamet, and F. Ciccacci, *Phys. Rev. B* **92**, 214403 (2015).
- ²⁷E. Saitoh, M. Ueda, H. Miyajima, and G. Tatara, *Appl. Phys. Lett.* **88**, 182509 (2006).
- ²⁸a. Dimoulas, P. Tsipas, A. Sotiropoulos, and E. K. Evangelou, *Appl. Phys. Lett.* **89**, 252110 (2006).
- ²⁹E. J. Loren, J. Rioux, C. Lange, J. E. Sipe, H. M. van Driel, and A. L. Smirl, *Phys. Rev. B* **84**, 214307 (2011).
- ³⁰K. Ando, M. Morikawa, T. Trypiniotis, Y. Fujikawa, C. H. W. Barnes, and E. Saitoh, *Appl. Phys. Lett.* **96**, 082502 (2010).
- ³¹K. Ando, M. Morikawa, T. Trypiniotis, Y. Fujikawa, C. H. W. Barnes, and E. Saitoh, *J. Appl. Phys.* **107**, 113902 (2010).
- ³²A. D. Rakić, A. B. Djurišić, J. M. Elazar, and M. L. Majewski, *Appl. Opt.* **37**, 5271 (1998).
- ³³D. E. Aspnes and a. a. Studna, *Phys. Rev. B* **27**, 985 (1983).
- ³⁴F. Bottegoni, A. Ferrari, S. Cecchi, M. Finazzi, F. Ciccacci, and G. Isella, *Appl. Phys. Lett.* **102**, 152411 (2013).
- ³⁵J. Rioux and J. E. Sipe, *Phys. Rev. B* **81**, 155215 (2010).
- ³⁶F. Bottegoni, M. Celebrano, M. Bollani, P. Biagioni, G. Isella, F. Ciccacci, and M. Finazzi, *Nat. Mater.* **13**, 790 (2014).
- ³⁷G. Isella, F. Bottegoni, A. Ferrari, M. Finazzi, F. Ciccacci, G. Isella, F. Bottegoni, A. Ferrari, M. Finazzi, and F. Ciccacci, *Appl. Phys. Lett.* **106**, 232402 (2015).
- ³⁸I. Žutić, J. Fabian, and S. Das Sarma, *Phys. Rev. B* **64**, 121201 (2001).
- ³⁹S. Birner, T. Zibold, T. Andlauer, T. Kubis, M. Sabathil, A. Trelakis, and P. Vogl, *IEEE Trans. Electron Devices* **54**, 2137 (2007).
- ⁴⁰R. Klix, W. Dittmann, and S. R., eds., *Lecture Notes in Computer Science* (Springer Verlag, Cambridge, MA, 1994).
- ⁴¹F. Pezzoli, L. Qing, A. Giorgioni, G. Isella, E. Grilli, M. Guzzi, and H. Dery, *Phys. Rev. B* **88**, 045204 (2013).